Surface Robots based on S-Isothermic Surfaces

Noriyasu Iwamoto[1], Hiroaki Arai[2], and Atsushi Nishikawa[3]

***Abstract*— Surface robots can have many applications due to multiple degrees of freedom. Accordingly, many open research questions arise due to the limited number of realized cases and insufficient theory foundation. For a surface robot that performs deformations with shear deformation, the inner product calculation in a local coordinate system on the robot generally depends on the shear angle. However, the shear angle cannot be accurately measured, making it difficult to control the robot with coordinate transformation. We present herein a geometric robot with coordinates that are as locally orthogonal as possible. This robot is embodied by adding thickness to a special circle group, called the S-isothermic surface. We propose the utilization of inverse kinematics in S-isothermic-surface robots and demonstrate the results of actual realization.**

I. Introduction

The research on surface-shaped robots [1] has many potential applications, including the development of shapeshifters that can transform into an arbitrary shape and use shape-dependent functions (Fig. 1(a)). Such composite functions depend not only on global shapes, as suggested by the leverage principle, but also on the local shape of each sub-function. Considering the examples of these functions, such cases involve an increase in the surface area of the intestinal villi or the cooling and water-repellent effects of fine uneven structures. The function integration that is yet to be realized has been proposed as a concept for modular robots. If we consider such a robot from a simplified viewpoint, we note that to realize a shapeshifter, it is only necessary to construct a surface robot that can represent the target object to be deformed. Even if the surface deformation can be easily modeled using a computer, many challenges that have not yet been addressed in research must be resolved to realize such a robot.

At present, attempts to develop surface robots mainly correspond to the proposals of feasible robots [2]-[5]. Several specific theories have been formulated accordingly. The examples of these theories include the forward kinematics for a robot that combines two continuum manipulators [6] and a lumped mass system model that relies on the robot material and thickness [7]. A robot with artificial muscle actuators arranged in a grid has also been constructed, and its kinematics has been reported [8].

The kinematic theory for surface robots is supposed be grounded on the continuous and discrete surface theories in mathematics because surfaces can be represented as a two-dimensional differentiable manifold. The following question arises: Are there robots suitable for the theories described in differential geometry? Exploring such robots can facilitate an understanding of the features of the geometric theories and enable the corresponding geometric analysis. The present study focuses on the orthogonality of a local coordinate system of a robot to explore this kind of robots. To do this, we utilize a special discrete surface, called a circle packing mesh (CPM) [9]. The CPM is a discretized surface by circles.

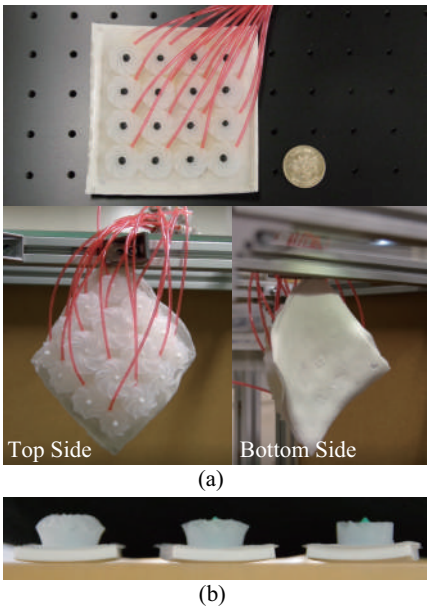

Fig. 1. Photographs (a) show an example of the S-isothermic surface robot proposed herein. This robot is composed of truncated conical actuators aligned in a grid shape and deformed by expanding the radii of the top side by applying pressure to the air chamber of each actuator, as shown in (b).

The deformation of surface robots (e.g., stretching a silicon rubber) generally includes shear deformation. Therefore, the local coordinate system set up on the robot is an oblique coordinate system with two coordinate axis angles dependent on the shear deformation. In this case, the shear angle appears in the formula for the inner product of the local coordinate system; however, accurately estimating the shear angle is difficult. Therefore, the development of a robot with orthogonal coordinates as a local coordinate system will result in easier control. The CPM deformation, in which the connection relationship does not change, is conformal; thus, the grid-like CPM in a Cartesian coordinate system keeps the orthogonality, even after a conformal deformation. In other words, robots based on the CPM are valid in terms of the

[1]Noriyasu Iwamoto is with the Faculty of Textile Science and Technology, Shinshu University, Ueda, Nagano, Japan iwamoto@shinshu-u.ac.jp

[2]Hiroaki Arai with the Department of Biomedical Engineering, Shinshu University, Ueda, Nagano, Japan

[3]Atsushi Nishikawa with Graduate School of Engineering Science, Osaka University, Toyonaka, Osaka, Japan

kinematic theory represented by differential geometry.

Robots based on the CPM can be realized in two ways: (i) enabling each circular actuator actively changing the radius; and (ii) considering that a contact point between actuators can be passively changed by the actuator radii. To realize such a robot, we proposed a truncated-cone actuator (Fig. 1(b)) to discretize a surface with a constant thickness [10] and a radius that could be modified on one side using the origami technology [11]. A robot based on the pseudo CPM could be realized by connecting the sides where the actuator radius does not change.

The present paper discusses the proposed robot in connection with an S-isothermic surface [12] that corresponds to a special CPM using the incircles of quadrilaterals. The remainder of this paper is structured as follows: Section III explains the developed numerical algorithm of inverse kinematics to explore the radii of the actuators realizing the shape of a given surface; and Section IV presents the proposed implementation method of an S-isothermic surface robot and the experimental results.

II. S-isothermic Surface Robots

A. Circle Packing Mesh

The CPM [13] refers to a mesh in which circles cover a closed area or in which circles are connected along a curve. The background of the CPM relies on Thurston's conjecture [14], in which infinitesimal circles can be used to approximate the Riemann mapping from a closed area onto a unit circle in $\mathbb{R}^2$ [15] that exhibits conformality. Accordingly, the conjecture has been proven, and numerical algorithms for identifying Riemann mappings using the CPM have been proposed [13]. When an area to be mapped is on a surface, a method for defining a conformal mapping needs to be based on texture mapping [15]. The conformal mappings in this context are referred to as discrete because the surfaces can be represented as discrete triangular surfaces using computer modeling.

Conformal mapping involves the deployment of infinitesimal circles onto infinitesimal circles, and therefore, often displays infinitesimal circles on a surface as a texture to verify the map conformality [16]. Let us consider a CPM with circles aligned in two directions in $\mathbb{R}^2$, as shown in the left part of Fig. 2, which are mapped onto a surface using map $\boldsymbol{f}$, as shown in the right part of Fig. 2. If map $\boldsymbol{f}$ has conformality, then in the CPM, the grid connecting the centers of the adjacent circles (solid line A in Fig. 2) and the grid comprising the common tangents of the adjacent circles (dotted line B in Fig. 2) remain orthogonal to each other after mapping. The combination of the solid and dotted curves in different directions also keeps the orthogonality after mapping by $\boldsymbol{f}$. If $\boldsymbol{f}$ is a quasi-conformal map, then the infinitesimal circles after mapping are elliptical.

In addition, far from the aforementioned purpose, the CPM is considered as a design method for arranging circles onto surface-shaped buildings and accessories. Schiftner et al. [9] proposed an algorithm for developing a CPM using the incircles of triangles with a rather straightforward procedure.

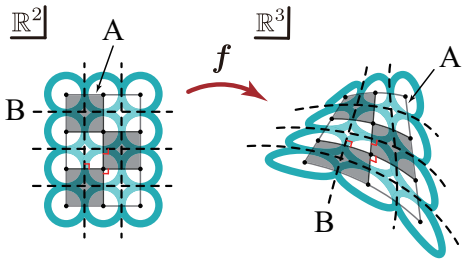

Fig. 2. Feature of a circle packing mesh with the lattice of circles. Here, the mesh is mapped onto a surface by conformal mapping. The conformal mapping exhibits a circle-circle correspondence such that the topology and the circular shape of the CPM are maintained on the mapped surface. The angles of the orthogonal grids (A and B) connecting the center of the circles and their contact points with the adjacent circles remain orthogonal on the surface.

First, the given continuous surface is divided by a triangular mesh. Next, all circles inscribed in each triangle of the mesh are derived. Subsequently, the tangent points of the circles on the triangular edges are computed. At this stage, the tangent points on the common edge of the adjacent triangles do not touch each other. Therefore, optimization is performed while updating the vertex positions of a triangular mesh such that the tangent points become close to each other.

B. S-isothermic Surface

Sechelmann et al. [12] proposed the concept of S-isothermic surfaces that discretized isothermic surfaces to the CPM using square incircles. Constructing a CPM using a quadrilateral mesh, the conditions under which a quadrilateral has an inscribed circle must be considered in addition to the condition for constructing a CPM using a triangular one. An S-isothermic surface can be constructed by satisfying the three following conditions: (i) the four vertices of a quadrilateral are on the same plane; (ii) an incircle touches all four edges of a quadrilateral; and (iii) two incircles of the neighboring quadrilaterals are in contact with the common edge.

Given three points, we consider the condition corresponding the fourth point with an incircle. Now, let the three-dimensional (3D) position vectors of three points be $\boldsymbol{v}_1$, $\boldsymbol{v}_2$, and $\boldsymbol{v}_3$, and let the other point be $\boldsymbol{v}_4$. Vector $\boldsymbol{d}_{ij} \in \mathbb{R}^3$ from vertex i to vertex j is denoted as $\boldsymbol{d}_{ij} = \boldsymbol{v}_j - \boldsymbol{v}_i$. First, for an incircle to exist, four points must be on the same plane. The condition can be expressed as follows considering four points as a tetrahedron:

$$\boldsymbol{d}_{21} \cdot (\boldsymbol{d}_{42} \times \boldsymbol{d}_{31}) = 0 \tag{1}$$

Furthermore, even if four points are in the same plane, there is not always a circle that can touch all four edges. The following must be satisfied considering the geometric relationship:

$$||\boldsymbol{d}_{21}|| + ||\boldsymbol{d}_{34}|| - ||\boldsymbol{d}_{23}|| - ||\boldsymbol{d}_{41}|| = 0. \tag{2}$$

Let the angle of vertex i corresponding to quadrilateral α be α_i and the angle of vertex i of the adjacent quadrilateral β

be β_i. For the four angles located at both ends of the edge shared by two quadrilaterals, the following condition holds assuming that the tangent points of the adjacent incircles match:

$$\cot\frac{\alpha_i}{2}\cot\frac{\beta_j}{2}-\cot\frac{\beta_i}{2}\cot\frac{\alpha_j}{2}=0. \tag{3}$$

The vertex positions of a quadrilateral mesh satisfying these conditions can be obtained by performing an optimization using the method proposed by Schiftner et al. [9]. However, the selection of an initial solution of the optimization is important in terms of its convergence. In [12], quasi-isothermal parameterization was applied to a triangular mesh with a higher resolution compared with a quadrilateral one. The result was used as an initial solution of the optimization algorithm.

C. S-isothermic Surface Robot

In this study, S-isothermic parameterization was performed as a method to construct surface robots. An actuator represented as a discretized element is a truncated cone-shape actuator with a constant thickness [10]. An S-isothermic surface robot has two surfaces: the bottom and top sides, respectively. Assume that the bottom and top sides of an actuator are parallel. When S-isothermic surfaces are used in the bottom side, they cannot be employed in the top side because twisting may occur between the actuators. As it can be seen from the discussion provided in Section II-A, the center point of the bottom side corresponding to each actuator and the contact point between the actuators lie on the curve obtained through conformal mapping from the orthogonal grid of $\mathbb{R}^2$ onto the bottom side.

To simplify the discussed concept, we assume herein that the truncated cone actuators are rigid. The controllable parameters are defined as the radii of the bottom and top sides of all actuators.

III. Inverse Kinematics

The inverse kinematics problem of an S-isothermic surface robot aims to identify the radii of the actuators used as the control parameters of a robot for a given surface. This problem formulation can be used not only for the original purpose, but also to determine the parameters in the implementation of an actual robot and to provide a non-divergent initial solution in a mechanical simulation.

Two problems are encountered when solving the inverse kinematics problem. First, S-isothermic parametrization cannot be realized analytically from a given discrete surface. Second, it is desirable that the actuators with thickness would be contacted at the edge of a truncated cone to form a connection relationship with the adjacent actuators. Therefore, we solve the inverse kinematics problem through numerical calculations. We propose an algorithm to do this.

A. Algorithm

To solve the inverse kinematics problem, numerical software programs must execute such functions as the S-isothermal parametrization of a given surface, minimization of contact point errors on the edges of adjacent truncated cone actuators, and displaying the obtained solution. It is also desirable to provide a possibility to adjust the design variables of the robot, such as the thickness and radius of each actuator and their number. Therefore, the algorithm was constructed herein using a 3D CAD system, Rhinoceros6, and Grasshopper.

The inputs to the entire algorithm are the target surface, number of actuators in the u and v directions, and actuator thickness. The radii on the bottom and top sides of each actuator r_i^b, r_i^t, position of the circle center on the bottom side $\boldsymbol{p}_i^b$, and rotation matrices of posture $\boldsymbol{M}_i$ are provided as the outputs. An S-isothermic surface for the bottom side of the robot was configured from the target surface to satisfy Eqs. (1)–(3). The position and the posture of the top side were obtained by incorporating the thickness based on the position and posture of the bottom side. Next, the radii of the top side were repeatedly modified by pseudo-optimization to set the contact points with adjacent actuators as close as possible to each other. The Daniel Piker's algorithm was adopted within the Grasshopper component to compute an S-isothermic surface [18].

B. Pseudo-optimization for Modification of the Top Side Radius

First, we derived error $e_{i,j}$ between the contact points of adjacent actuators i and j. If the center position of the top side of the actuator $*$ is expressed as $\boldsymbol{p}_*^t$, then vector $\boldsymbol{v}_{i,j}$ from the center of the top circle of actuator i to that of actuator j is defined as $\boldsymbol{v}_{i,j}=\boldsymbol{p}_j^t-\boldsymbol{p}_i^t$. Let the normal vector of the top side in the actuator $*$ be $\boldsymbol{n}_*$. In this case, the position of a contact point can be expressed as follows because the contact point of actuator i is located on its top circumference: $\boldsymbol{p}_{i,j}^i=r_i^t(\boldsymbol{n}_i\times\boldsymbol{v}_{i,j})\times\boldsymbol{n}_i$. We define the sgn function as follows:

$$\mathrm{sgn}(x)=\begin{cases}1 & (x\geq 0)\\ -1 & (x<0)\end{cases},$$

The error $e_{i,j}$ between the contact points can be calculated as follows:

$$e_{i,j}=\mathrm{sgn}(\boldsymbol{v}_{i,j}\cdot\boldsymbol{n}_i)\ \|\boldsymbol{p}_{i,j}^j-\boldsymbol{p}_{i,j}^i\|.$$

In the case of $e_{i,j}<0$, the two actuators are considered as intersecting. In the case of $e_{i,j}=0$, the top circles of the two actuators are touching each other.

The energy function of each actuator is defined as follows based on the error between each contact point:

$$E_i=\sum_j\frac{1}{2}e_{i,j}^2. \tag{4}$$

We then modify the top radii of all actuators such that their total energies $\sum_i E_i$ are minor.

An effective method involves the usage of a well-known optimization method. However, in this study, we implemented pseudo-optimization as a simple method. The modified top radius r'^t_i was calculated according to the updating

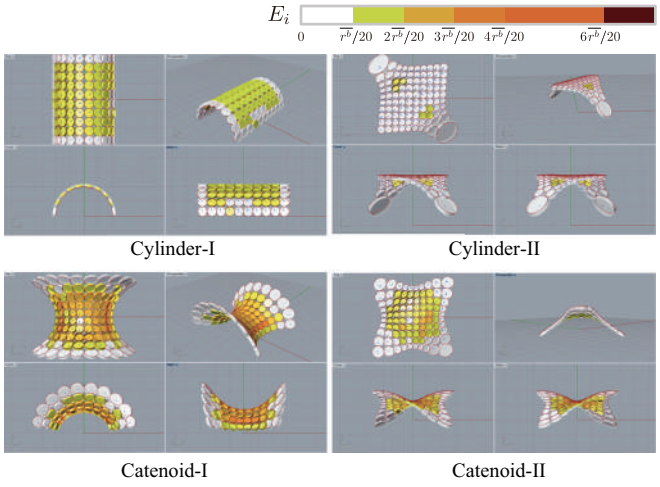

Fig. 3. Results of applying the proposed algorithm to the cylindrical and catenoid surfaces. Each actuator is colored according to the value of the energy function E_i, which indicates the degree of contact points with the neighboring actuators on the top side. The white color indicates the case with the least energy. The value of the energy function considerably differs when cutting the rectangular mesh for a given surface and if the mesh is cut such that the gaps between the actuators are arranged in the principal curvature direction. Accordingly, E_i becomes small.

rule using coefficients ω, λ:

$$\begin{aligned} D_i &= \sum_j w_{i,j} e_{i,j} \\ r'^t_i &= r^t_i - D_i/\lambda \end{aligned}$$

Energy E_i can be reduced by applying this modification. The weights $\omega_{i,j}$ are set as follows:

$$\omega_{i,j} = \begin{cases} \omega_S & (e_{i,j} > 0) \\ 0 & (e_{i,j} = 0) \\ \omega_F & (e_{i,j} < 0) \end{cases}$$

using a positive constant ω_S and a negative constant ω_F.

C. Results

The results of the inverse kinematics performed on a cylinder and a catenoid surface are discussed herein. In Fig. 3, the actuators with a small energy (Eq. (4)) are displayed in white, while those with a large energy are represented by six stages in dark colors. Based on the average value of the bottom radius $\overline{r^b} = \sum_i r^b_i/N$ (N is the number of actuators), the five thresholds were set to $\overline{r^b}/20$, $2\overline{r^b}/20$, $3\overline{r^b}/20$, $4\overline{r^b}/20$, and $6\overline{r^b}/20$ in order of increasing.

When a continuous surface is discretized by a quadrilateral mesh, several methods can be considered depending on a direction. Cylinder-I and Catenoid-I in Fig. 3 represent the cases in which the mesh is cut along the principal direction. Cylinder-II and Catenoid-II correspond to the case in which the mesh is cut in the direction rotated by 45° from the principal direction. The latter resulted in a smaller number of errors compared to the former. The principal direction denotes the direction of the maximum and minimum curvatures at a given point. The simulation results indicate that it is difficult to reduce the error for the contact points corresponding to the principal direction with respect to the center of an actuator. The actuators with a low energy can be regulated by arranging the principal direction to a gap generated when the four truncated cone actuators are connected. Fig. 4 outlines the result of applying the considered algorithm to a complex target surface. If S-isothermic parameterization cannot be applied to the target surface, an S-Isothermal parameterized surface is constructed with a shape as close as possible to the target one. In this way, we can obtain the result, as represented in Fig. 4.

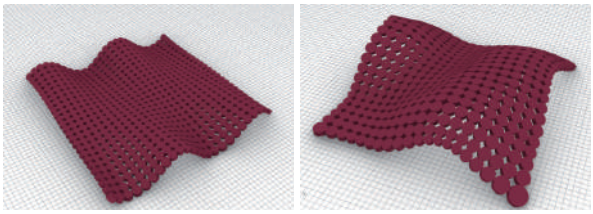

Fig. 4. Results of solving the inverse kinematics problem for two complex geometries using the proposed algorithm. S-isothermic surface robots can represent these surfaces accurately if the number of actuators is appropriately set.

IV. Realization

A. Components of the Proposed Robot

The S-isothermic surface robot proposed in this study was composed of the pneumatic truncated cone actuators (Fig. 1(b)) aligned in a grid pattern. The number of actuators was set to 16 and arranged in a square 4×4 grid, such that the robot becomes symmetrical, and the production cycle is sped up. The 16 actuators were integrally formed by pouring silicon into a mold. A single actuator was constructed with a top-lateral part, a pillar, a bottom part, and an air tube. The top side of each actuator had the folded part. The lateral side was the side wall of the actuator. The bottom side was implemented as the base sheet (Fig. 5). The folded structure at the top side enabled the actuator to expand evenly in the radial direction and prevented it from deforming in the thickness direction as much as possible[10]. In the same manner, the center pillar was intended to suppress the expansion in the thickness direction. Ecoflex$^{\mathrm{TM}}$ 00-50 rubber (platinum-catalyzed silicon) was selected as the silicon material for realizing the top-lateral part due to its softness, toughness, and deformability. Wave silicone rubber (Wave Co., Ltd.) corresponding to hardened silicone was adopted as the material of the bottom part to prevent the expansion to the bottom side and recover the natural shape during decompression.

B. Automatic 3D Modeling of the Silicon Mold

The silicon molds were designed using the CAD software tools, Rhinoceros6 and Grasshopper, to adjust the design variables (e.g., number of actuators and the thickness of silicon rubber). We considered three types of molds, namely male and female molds for the top-lateral part (Fig. 5(a)), and bottom molds for the bottom part. The two types corresponding to the top-lateral part were created by meshing

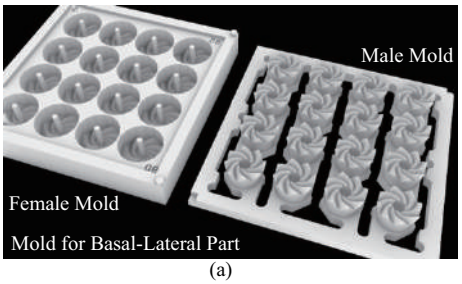

(a)

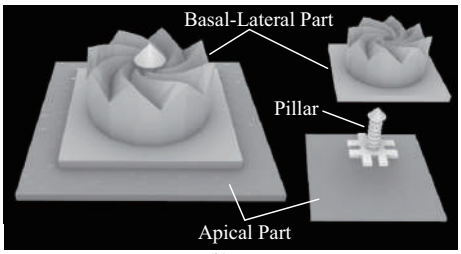

(b)

Fig. 5. (a) Molds for casting the top-lateral side of the actuator. Considering the number of actuators and the silicon thickness, a 3D mold model is automatically generated by Rhinoceros 6 and Grasshopper. (b) Structure of a single actuator. The actuator comprises three components: top-lateral side (soft silicon), bottom side (hard silicon), and pillar made of ABS resin.

using Grasshopper based on the 3D positions of the vertices of a folded structure obtained according to [10]. In this case, the diameter of the folded part of the female mold (outside wall of the actuator) was set to 20 mm. Concerning the male model (inside wall of the actuator), the reduction ratio must be determined according to the set appropriate thickness. The folded part of the male model must be rotated by an extent proportional to the reduction ratio. This was required because the silicon rubber thickness was not constant when the model was generated without rotation. The foundation of the central pillar formed a # shape. The degree of conjunction through silicon was increased due to the penetration of silicon into the gaps in the foundation. The side of the central pillar had a wave structure with a sinusoidal wave rotated around the central axis, which allowed increasing the frictional force while using silicon. The silicone molds and the core column were fabricated with ABS resin using a 3D printer.

C. Production

The procedure for implementing the robot is specified below. First, the top-lateral part was fabricated by casting silicon into its male and female molds. Before the silicon hardened, it was placed in a vacuum for approximately 20 min such that no bubbles remained. It was then left in a 50°C thermostatic bath for approximately 30 min. After removing the molds from the thermostatic bath, they were extracted, and the top-lateral part was completed. Next, hard silicon was poured into the bottom mold, and the top-lateral part, in which the tube and the heart central pillar were inserted, was placed on the bottom mold until the hard silicon seizes to harden. Subsequently, the robot was considered as completed. As a result of the trial-and-error tests, a pneumatically driven robot composed of 4×4 actuators with the top surface thickness of 0.1 mm and a male reduction ratio of 0.8 was fabricated (Fig. 1). The total size of the robot was approximately 100 mm square.

D. Actuation

In this experiment, a microcontroller (Arduino Mega 2560) was used to send analog signals to the regulators (SMC ITV00-30-2ML) via a DA converter to set the pressure. Simultaneously, the solenoid valves (SMC S070C-5DC-32) were controlled by sending an ON-OFF signal from the microcontroller to the MOSFET switches. When the solenoid valves were opened, the pressures set in the regulators were applied to the inside of the actuator chambers. The simple step signals were set to the regulators in the experiment to confirm the robot deformation. We prepared two patterns for pressure application to the actuator (Figs. 6(a) and (b)).

Fig. 7 shows the deformation of the pattern (a) in Fig. 6 when the air pressure was increased by 1 kPa per second. A pressure of 15$\sim$40 kPa was applied to the 12 actuators, except for the four of them that were in the corners. Fig. 1 illustrates an enlarged photo of the deformation shape at 40 kPa. The folded structure of the top side expanded according to the set pressure. The adjacent actuators pushed against each other such that the entire surface was bent. From the pressure pattern of the actuators, we predicted that the robot will be spherical, but the obtained deformation showed that the bottom corner deformed less than the left and right ones. We assumed that the main reason for this result is that the air tubes prevented the robot from deforming. The pressure could not be set higher than 40 kPa because of the softness of the silicone rubber material. The influence of the air tube is expected to become weaker when the softness is optimized, and a higher pressure is set. Fig. 6(c) shows the deformation results of pattern (b) at 40 kPa. In pattern (b), the robot was deformed into a cylinder because it was applied to the actuators on two opposite edges at the boundary. However, the drive pattern was different from the Cylinder-I radius pattern in Fig. 3 obtained by inverse kinematics, which may be due to the small number of actuators for realizing a cylinder. By increasing the number of actuators and reducing the amount of change in each actuator, the drive pattern was expected to be closer to the radius pattern of Cylinder-I. The circle-circle correspondence of conformal mapping in Section II-A can be observed on the top side of the robot. This result means that if we can observe one side of the robot with an external camera, we can visually estimate the robot coordinates set based on the quasi-isothermic properties.

V. Conclusion

This study proposed the concept of a surface robot with the kinematics comprising multiple truncated conical actuators. We described herein the realization of the proposed robot and the results of the conducted pneumatically driven experiments. One side of the robot was specially realized as a surface, called S-isothermic surface, made from circles. Considering the inverse kinematics concept, we proposed a method for estimating the radii of two sides through

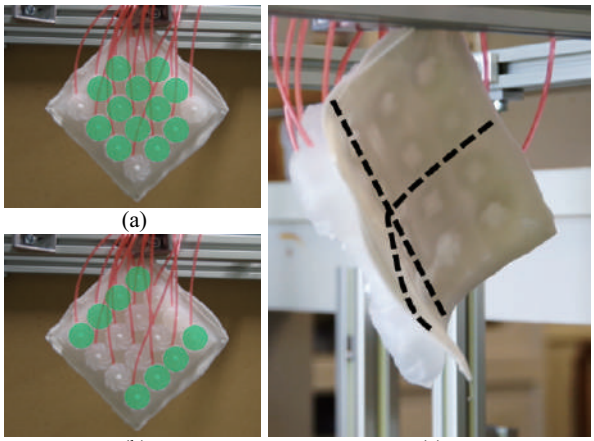

Fig. 6. Photographs in (a) and (b) represent two driving patterns with the same pressure set for the actuators marked in green. All actuators, except for the four corner actuators, are launched in the pattern in (a). The results of this pattern are depicted in the picture below Fig. 1. The actuators located in the upper left and lower right rows of the actuators located at the edges are launched in the pattern in (b). The result of this pattern is provided in (c).

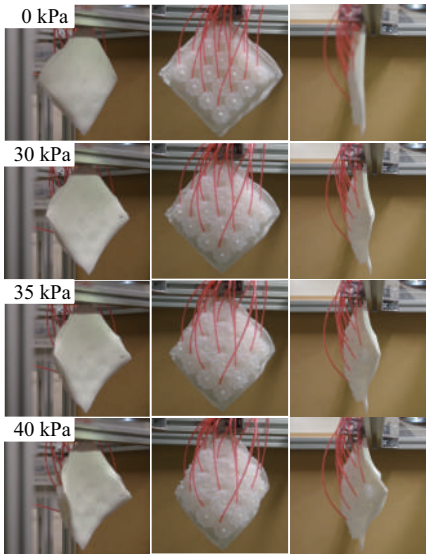

Fig. 7. Results of driving the actuator in the pattern, as shown in Fig. 6(a) for the proposed S-isothermic surface robot. The internal pressure is gradually applied to the actuator from 15 kPa to 40 kPa.

S-isothermic parameterization and pseudo-optimization for adjacent points. Furthermore, a silicon rubber mold was automatically generated by a specific program, and a robot composed of 4×4 actuators was realized accordingly.

The obtained results are the first step toward the realization of a robot that can obtain a Cartesian coordinate system as a local coordinate system. The further development of this robot will enable us to apply the geometric theory to it. The conformal parameterization to discrete surfaces has been used in texture mapping in computer graphics, and many algorithms for editing the surfaces have been developed. It is expected that the editing algorithm can be introduced to robotics.

However, the results of the present research still presented many challenges. For example, the kinematics concept proposed herein does not imply supporting singularities. Therefore, the parameterization quality is actually low, even for the surfaces that can be realized through the S-isothermic ones. Supporting singularities can facilitate the realization of more accurate S-isothermic surfaces; however, the connection between actuators must still be modified.

REFERENCES

[1] I. D. Walker, "Continuum Robot Surfaces: Smart Saddles and Seats", Mechatronics and Robotics Engineering for Advanced and Intelligent Manufacturing, 2017, pp 97 - 105, 2017

[2] D. Rus and M. T. Tolley, "Design, fabrication and control of origami robots", Nature Reviews Materials, vol. 3, pp. 101-112, 2018.

[3] E. Steltz, A. Mozeika, N. Rodenberg, E. Brown and H. M. Jaeger, "JSEL: Jamming Skin Enabled Locomotion", Proceedings of the IEEE/RSJ International Conference on Intelligent Robots and Systems, 5672-5677, 2009.

[4] R. Sirohi, Y. Wang, S. Hollenberg, I. S. Godage, I. D. Walker, and K. E. Green: "Design and Characterization of a Novel, Continuum-Robot Surface for the Human Environment", *IEEE 15th International Conference on Automation Science and Engineering*, 2019.

[5] Y. Wang, C. Frazelle, R. Sirohi, L. Li, I. D. Walker, and K. E. Green: "Design and Characterization of a Novel Robotic Surface for Application to Compressed Physical Environments", *International Conference on Robotics and Automation 2019*, 2019.

[6] J. Merino, A. L. Threatt, I. D. Walker, and K. E. Green: "Forward Kinematic Model for Continuum Robotic Surfaces", Proceedings of the IEEE/RSJ International Conference on Intelligent Robots and Systems, pp. 3453-3460, 2012.

[7] H. Habibi, R. Kang, I. D. Walker, I. S. Godage, and D. T. Brason: "Developing a 3-D, Lumped-Mass Model to Present Behavior of Large Deformation Surface Based Continuum Robots", IUTAM Symposium on Intelligent Multibody Systems – Dynamics, Control, Simulation, pp. 133-147, 2019.

[8] O. Medina, A. Shapiro, and N. Shvalb: "Minimal Actuation for a Flat Actuated Flexible Manifold", IEEE Transaction on Robotics, vol. 32, no. 3, pp. 698-706, 2016.

[9] A. Schiftner, M. Höbinger, J. Wallner, and H. Pottmann, "Packing Circles and Spheres on Surfaces", *ACM Transaction on Graphics*, vol. 28, Issue 5 (2009), Article No. 139, pp.1-8.

[10] Yang Jiang, Atsushi Nishikawa, and Noriyasu Iwamoto, "Design and Fabrication of a Deployable Rubber Membrane for a Circular Mesh-Type Robot", *Proceedings of the 15th International Conference on Control, Automation, Robotics and Vision*, (2018), pp.1-6.

[11] S. Ishida, T. Nojima and I. Hagiwara, "Design of Deployable Membranes Using Conformal Mapping," vol.19-4, *Transaction of ASME, Journal of Mechanical Design*, vol. 137, issue 6, 2015.

[12] S. Sechelmann, T. Rörig, and A. I. Bobenko, "Quasiisothermic Mesh Layout", Advances in Architectural Geometry, (2012), pp 243-258.

[13] K. Stephenson: "Introduction to Circle Packing: The Theory of Discrete Analytic Functions", *Cambridge University Press*, 2005.

[14] William Thurston, "The
Finite Riemann Mapping Theorem" , *Invited talk, An International Symposium at Purdue University on the occasion of the proof of the Bieberbach conjecture*, (1985).

[15] L. Kharevych, B. Springborn, P. Schröder: "Discrete Conformal Mappings via Circle Patterns", *ACM Transactions on Graphics*, vol. 25, no. 2, pp. 412-438, 2006.

[16] H. Zhao, X. Li, H. Ge, N. Lei, and X. Gu: "Conformal Mesh Parameterization Using Discrete Calabi Flow", *Computer Aided Geometric Design*, vol. 63, pp. 96-108, 2018.

[17] M. P. do Carmo, "Differential Geometry of Curves & Surfaces", Dover Publications, 2016.

[18] https://discourse.mcneel.com/t/ellipsoid-mesh-from-curvature-lines/81480/2